PCCP

PAPER

View Article Online
View Journal | View Issue

Cite this: *Phys. Chem. Chem. Phys.*, 2017, **19**, 28928

First-principles study of Ga-vacancy induced magnetism in β-Ga_2O_3†

Ya Yang,[a] Jihua Zhang,[b] Shunbo Hu,[c] Yabei Wu,[a] Jincang Zhang,[ac] Wei Ren *[ac] and Shixun Cao *[ac]

Received 1st June 2017,
Accepted 2nd October 2017

DOI: 10.1039/c7cp03675b

rsc.li/pccp

First principles calculations based on density functional theory were performed to study the electronic structure and magnetic properties of β-Ga_2O_3 in the presence of cation vacancies. We investigated two kinds of Ga vacancies at different symmetry sites and the consequent structural distortion and defect states. We found that both the six-fold coordinated octahedral site and the four-fold coordinated tetrahedral site vacancies can lead to a spin polarized ground state. Furthermore, the calculation identified a relationship between the spin polarization and the charge states of the vacancies, which might be explained by a molecular orbital model consisting of uncompensated O^{2-} 2p dangling bonds. The calculations for the two vacancy systems also indicated a potential long-range ferromagnetic order which is beneficial for spintronics application.

1 Introduction

d^0 ferromagnetism has attracted great attention, ever since it was reported by Coey in a review on materials with an absence of partially filled d or f shells.[1] For instance, there appeared an unexpected magnetism in a HfO_2 film with a Curie temperature exceeding 500 K and a magnetic moment of about 0.15 bohr magnetons per formula unit.[2] In contrast to dilute ferromagnetic semiconductor oxides, it is amazing that ferromagnetism was discovered in HfO_2,[2–5] ZnO,[6–8] GaN,[9–14] Fe-substituted In_2O_3[15] and TiO_2.[16–18] As is well known, the traditional approaches to magnetism in solids are based on local moments, or on electrons delocalized in narrow energy bands. Without magnetic ions, the lattice defects may be the alternative key.[2] The neutral and charged point-defects in inorganic or organic systems have been studied for a long time by quantum chemical and density functional theory methods.[19–28] The cluster model, supercell model and embedded-cluster model have been successfully employed to investigate the properties of oxygen-vacancies in CeO_2[22] and MgO.[25–27] Researchers have identified that vacancies should be responsible for the amazing magnetism in nonmagnetic systems due to the oxygen-vacancy induced unpaired spin localization. Weng *et al.*[3] have shown that hole doping in the oxygen p orbital of HfO_2 can induce ferromagnetism and this may be a general phenomenon in ionic oxides. A similar effect was also already found in CaO for cation vacancies.[29] It is reasonable to believe that the intriguing magnetism originates from intrinsic lattice defect states like vacancies, and such results suggest a new way to change the magnetic states of the semiconductors without doping.

As a widely used material in the semiconductor industry, at room temperature the stable state β-Ga_2O_3 has a wide band gap of about 4.4–4.8 eV. Due to this, β-Ga_2O_3 has a unique transparency from the visible into the UV (ultraviolet) region, thus being a good candidate for optoelectronic devices.[30] However, Ga_2O_3 is nonmagnetic due to the $3d^{10}$ configuration of the Ga^{3+} ions which limits its use in spintronics. Recently, bulk ferromagnetism was found experimentally in Ga_2O_3, together with large changes in photoluminescence intensity induced by a magnetic field.[31] The authors claimed that magnetism could be formed locally around the special site of oxygen vacancies and for some vacancy densities the magnetism could correspond to the experimental results. Some previous theoretical reports have studied the vacancies and ion doping effect in β-Ga_2O_3, but no one has shown magnetism explicitly.[32–34] Based on the research studies on other semiconductors,[2–18] most reporters have identified that cation vacancies should be responsible for the d^0 ferromagnetism. Recently, some effects of the intrinsic Ga- and O-defects were investigated in pure and aluminum-doped β-Ga_2O_3 using the GGA+*U* (generalized gradient approximation plus Hubbard *U*) method.[35,36] It is noteworthy that the GGA method may fail to describe systems with d and f electrons, which results in underestimation of the band gap. In β-Ga_2O_3, the GGA+*U* method has been proved to reproduce reasonable values of the band gap close to those of experiments.

[a] *Department of Physics, and International Center of Quantum and Molecular Structures, Materials Genome Institute, Shanghai University, Shanghai 200444, China. E-mail: renwei@shu.edu.cn, sxcao@shu.edu.cn*
[b] *Guizhou Provincial Key Laboratory of Computational Nano-Material Science, Guizhou Education University, Guiyang 550018, China*
[c] *Shanghai Materials Genome Institute, Shanghai, 200444, China*

† Electronic supplementary information (ESI) available. See DOI: 10.1039/c7cp03675b

But until now, a microscopic theoretical investigation of the cation-vacancy-induced magnetism in β-Ga_2O_3 has been lacking. And considering the tetrahedral and octahedral sites of Ga atoms in β-Ga_2O_3, the possible local clusters induced by the Ga-vacancies would be polarized by the charges, which may facilitate a stable ferromagnetic order.[37,38] We test the possible cation vacancies using spin-polarized density functional theory (DFT) calculations. The GGA+U approach is used to get a reasonable electronic structure and spin alignment. And we adopted molecular orbital theory to understand and predict the magnetic behaviors. Therefore, compared to ferromagnetic metals and other nonmagnetic semiconductors, our calculation aims to reveal the origins of the unexpected magnetism appearing in β-Ga_2O_3 and open an avenue for the development of the β-Ga_2O_3 applied in the integration of spintronics and semiconductor-based electronics.

2. Computational method

Spin-polarized DFT calculations were performed by using the Vienna ab initio simulation package (VASP) with the projector augmented wave (PAW) method.[39–42] The generalized gradient approximation (GGA) of Perdew–Burke–Ernzerhof (PBE) was used as the exchange and correlation functional.[43,44] The effective Hubbard energy ($U_{eff} = U - J$) was used to describe the electron correlation effect and produce an energy gap (4.2 eV) close to the experimental value (4.9 eV)[30] with a U_s = 30.0 eV for Ga-4s and U_p = 8.5 eV for O-2p. The electronic configurations $3d^{10}4s^24p^1$ and $2s^22p^4$ are considered as the valence states for Ga and O, respectively. It is noted that our U values are different from the ones in ref. 35 although the Hubbard U applied on the Ga-s orbital was just to open the energy gap (see more details in the ESI†).[45,46] The plane wave cutoff energy is 500 eV. For the bulk β-Ga_2O_3 and the vacancy-defect structures we adopted and optimized the experimental structures by keeping the lattice parameters unchanged until the forces on the atoms become less than 0.001 eV $Å^{-1}$. The following experimental values are used in our calculation of β-Ga_2O_3, a = 12.214 Å, b = 3.037 Å, c = 5.798 Å and β = 103.830° and the space group is $C2/m$.[47] The k-points were set with a Monkhorst–Pack mesh of 6 × 6 × 6. The tetrahedron method with Blöchl corrections[48] was used. In the electronic structure calculations, we use 10^{-6} eV for the energy convergence criterion. We then calculated the magnetic moment and density of states with the more accurate but computationally demanding HSE06 hybrid functional[49,50] (see more details in the ESI†).

3. Results and discussion

3.1 The structure optimization and the vacancy formation energy

We first use the DFT-GGA method to optimize the 60-atom supercell $Ga_{24}O_{36}$ and the $Ga_{23}O_{36}$ supercell containing a single gallium vacancy (V_{Ga}) in two different symmetry sites. As shown in Fig. 1, the Ga atoms have two symmetry sites (*e.g.*, four-fold and six-fold coordinated sites). For convenience of discussion, we name the four-fold coordinated vacancy as V^{tetra}, and the six-fold one as V^{octa}. In the situations of perfect local symmetry, the four-fold site constructs a tetrahedron with a group of T_d symmetry and the six-fold site builds an octahedron with a group of O_h symmetry. However, in the monoclinic crystal structure of the β-Ga_2O_3 the local geometry of the coordinated anions around the gallium has a distortion of the perfect symmetry. The relaxed structural details are shown in Fig. 1(b) and (c), where the GaO_6 octahedron has two pairs of bonds of equal length in the basal plane and two different bonds along the long axis of the octahedron; whereas the GaO_4 has two equal-length bonds among the four Ga–O bonds. It is also worth noting that the bond angles of the O–Ga–O also have a significant deviation from perfect symmetric values. Hence, the distorted bonds and bond angles are expected to have an impact on the electronic structure of the systems with Ga vacancies.

After identifying the structure including the defect distortion, we calculated the vacancy formation energy (E_{vf}) at the two different sites $V^{octa,tetra}$ with several possible charge states (neutral, −1, −2 and −3) as defined in ref. 51:

$$E_{vf}[V^{octa,tetra}] = E_{tot}[V^{octa,tetra}] - E_{tot}[bulk] + \sum n_i\mu_i + q(E_F + E_{VBM}) \quad (1)$$

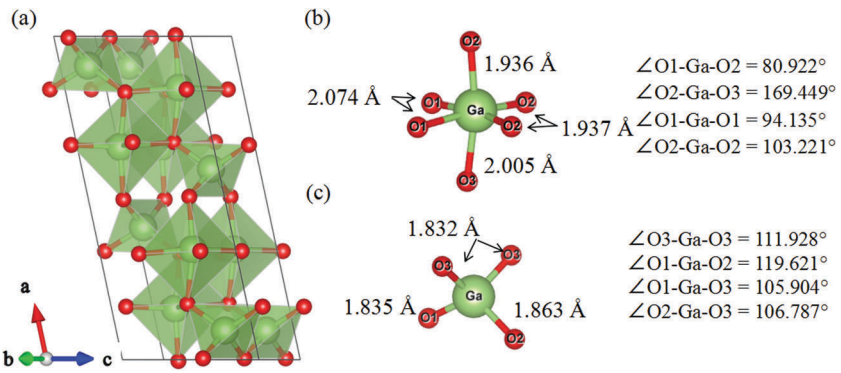

Fig. 1 (a) Crystal structure of the pure β-Ga_2O_3. (b) The local structure of the six-fold coordinated Ga–O octahedron and (c) the four-fold coordinated Ga–O tetrahedron. The green and red balls represent the Ga and O atoms, respectively.

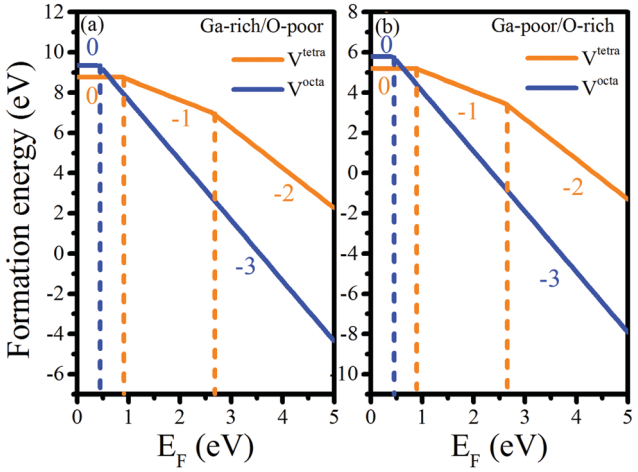

Fig. 2 Formation energies of V^{tetra} and V^{octa} Ga vacancies in various charge states as functions of the Fermi energy (a) for the Ga-rich environment and (b) for the Ga-poor environment.

where the E_{tot}[bulk] and $E_{tot}[V^{octa,tetra}]$ represent the total energies of the perfect supercell and that containing a vacancy in the charge state q. The integer $n_i = 1$ indicates the number of atoms that have been removed from the supercell to form the vacancy defect. The chemical potential μ_i of μ(Ga) is suggested to be equal to the bulk values for the corresponding metal in a Ga-rich/O-poor environment, and the E_F denotes the Fermi energy and varies between the valence band maximum (VBM) and conduction band minimum (CBM). In a Ga-poor/O-rich environment, $2\mu(Ga) = \mu(Ga_2O_3) - 3\mu(O)$, where $\mu(Ga_2O_3)$ is given by the energy of a formula unit of Ga_2O_3 and μ(O) by half of the energy of an O_2 molecule. In Fig. 2(a) and (b), we present the Ga-vacancies with −3, −2, −1 and 0 charge states as functions of the Fermi energy E_F. The results confirm that the four-fold coordinated V^{tetra} is more energetically preferable for neutral cation vacancies. As we discuss later for evidence of the magnetism induced by the cation vacancy in β-Ga_2O_3, both defects can introduce spin-polarized states with magnetic moments of 0.685 μ_B for V^{tetra} and 2.034 μ_B for V^{octa}. However, the relatively small stability of the V^{tetra} neutral 0 state is seen in a narrow range of the Fermi energy E_F, and upon increasing E_F the −3 state of V^{octa} becomes the most stable one. A similar case occurs in the Ga-poor/O-rich environment but with overall smaller formation energy. Although the −3 state of V^{octa} has a wide-range stability, it would actually suppress the vacancy induced ferromagnetism. Nevertheless, if the Fermi level is set close to the VBM and deep of the gap (*e.g.*, by connecting a metal contact)[52,53] the neutral V^{tetra} would be energetically preferred for formation of a large local magnetic moment.

3.2 The electronic structure

Then the electronic structures of the pure and vacancy systems were calculated as shown in Fig. 3(a)–(d). The pure Ga_2O_3 without vacancies has a nonmagnetic state with a gap of 4.2 eV at the GGA+U level close to the experimental value of 4.9 eV. (We have also tested the gaps with different U values as shown in the ESI.†) In addition, the total density of states (TDOS) of the $V^{octa,tetra}$ configurations are also shown in Fig. 3(a) exhibiting two different defect-states. In detail, for the V^{octa} a half-metal-like state

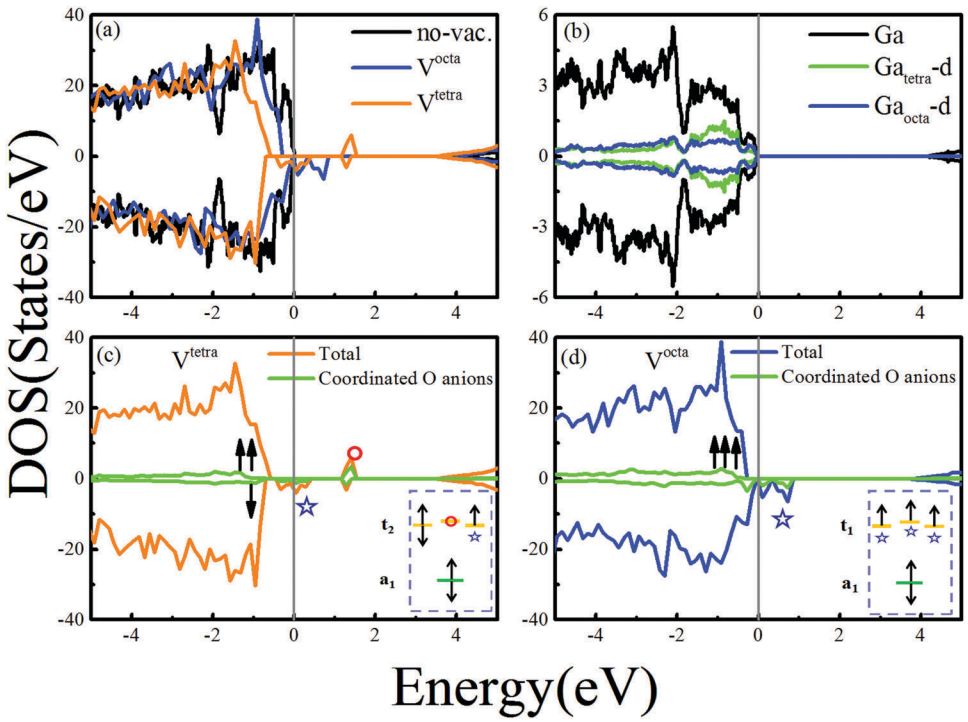

Fig. 3 (a) Total DOS of pure β-Ga_2O_3, and systems with V^{tetra} and V^{octa}. (b) Projected DOS of pure β-Ga_2O_3. (c) Projected DOS of V^{tetra}. (d) Projected DOS of V^{octa}. The vertical lines denote the Fermi level at 0 eV.

can be found around the Fermi level. In the V^{tetra} system, defect states are located inside the band gap for both spin up and spin down electrons. In Fig. 3(b) we give the projected density of states (PDOS) of the Ga ions in the pure Ga_2O_3 onto two coordination sites of tetrahedral and octahedral symmetries. Furthermore, from inspection of the PDOS for the vacancy systems shown in Fig. 3(c) and (d), it can be confirmed that the defect states are formed by the coordinated O-2p orbitals. Therefore, it is necessary to explain the vacancy properties by constructing the molecular orbitals based on the coordinated O-2p states.

Before analysing the molecular orbitals, we look at the spin charge density in Fig. 4. It is clear to see that the dangling bonds of the coordinated O anions create local magnetic moments with the shape of 2p orbits. Simultaneously, some next nearest neighboring O anions also have small moments possibly for the extended tails of the defect wave functions.[54] It is interesting to see that the dangling bonds almost point to the vacancy center for the s–p hybridization. However, we also note that some coordinated O anions contribute very little spin moments as indicated by the spin density distribution. Furthermore, the spin charge density tends to distribute mostly at the high symmetry sites of O anions bonded by the originally equal Ga–O bonds. A similar phenomenon was also found in HfO_2 with Hf-vacancies where the spin charge density will clump mainly on one of the two kinds of coordinated O atoms whereas another kind of O atom loses most of its spin polarization.[4] Therefore, the distributions of the spin charge agree with the distortion of the local vacancy structure and indicate a disturbance to the molecular orbitals. Next, we will explain the distinct properties of the V^{tetra} and V^{octa} hiding in the different symmetries.

3.3 The molecular orbital theory approach

Let us begin from the neutral Ga vacancy situation. Both the neutral V^{tetra} and V^{octa} would introduce electrons into the molecular orbitals formed by the coordinated O anions. The reasonable molecular orbitals will lead to a direct introduction of the behaviors of the defect states. For the perfect V^{tetra}, the nearest four O anions form a local environment with T_d symmetry. Under this T_d symmetry, based on the group theory[8] the linear combination of the p orbitals will result in a lowest energy level which is a single a_1 molecular orbital and a high energy level with a triple degenerate t_2 molecular orbital. All the possible states originate from the irreducible representations of the tetrahedral group T_d, for example:

$$a_1:\ v = \frac{1}{2}(\psi_1 + \psi_2 + \psi_3 + \psi_4) \quad (2)$$

$$t_2:\ t_x = \frac{1}{2}(\psi_1 + \psi_2 - \psi_3 - \psi_4) \quad (3)$$

$$t_y = \frac{1}{2}(\psi_1 - \psi_2 - \psi_3 + \psi_4) \quad (4)$$

$$t_z = \frac{1}{2}(\psi_1 - \psi_2 + \psi_3 - \psi_4) \quad (5)$$

where ψ_1 is expressed as a function of the atomic orbitals, $\psi_1 = (s + p_x + p_y + p_z)$ corresponding to the four dangling bonds pointing towards the vacancy site and the other three orbitals are given as ψ_j (j = 2, 3, 4). Chanier *et al.* have used this sp^3 molecular orbital model to explain the cation vacancies in ZnA (A = S, Se, Te).[8]

Analogously, the perfect V^{octa} coordinated symmetry belongs to the O_h group. According to the irreducible representations of the octahedral group O_h, we could also get two molecular orbitals (a_1 and t_1) similar to the V^{tetra} as shown in Fig. 5(a) and (e). For example:

$$a_1:\ v = \frac{1}{\sqrt{6}}(\psi_1 + \psi_2 + \psi_3 + \psi_4 + \psi_5 + \psi_6) \quad (6)$$

$$t_1:\ t_x = \frac{1}{\sqrt{2}}(\psi_1 - \psi_2) \quad (7)$$

$$t_y = \frac{1}{\sqrt{2}}(\psi_3 - \psi_4) \quad (8)$$

$$t_z = \frac{1}{\sqrt{2}}(\psi_5 - \psi_6) \quad (9)$$

the ψ_j (j = 1, 2, 3, 4, 5, 6) are corresponding to the six coordinated O atoms.

But it is very important to point out the difference between V^{tetra} and V^{octa}. The breaking of the local vacancy structure symmetry results in different Ga–O bonds and a heterogeneous spin charge density distribution. One state of the three t orbitals would be lifted to a higher energy state, such that the t level is divided into lower doubly degenerate e levels and a higher singlet b level. Then, we use the SymApps software[55] to confirm the local symmetry of the relaxed vacancy structure. Based on the distorted local structure and applied group theory, it is convenient to construct the new molecular orbitals. As shown in Fig. 6, by taking off the central Ga^{3+} ions the local structure will be distorted away from the perfect symmetry of the O_h group for the V^{octa} and reduced to a D_{2d} group; the T_d group of the V^{tetra} will be reduced to a S_4 one. According to

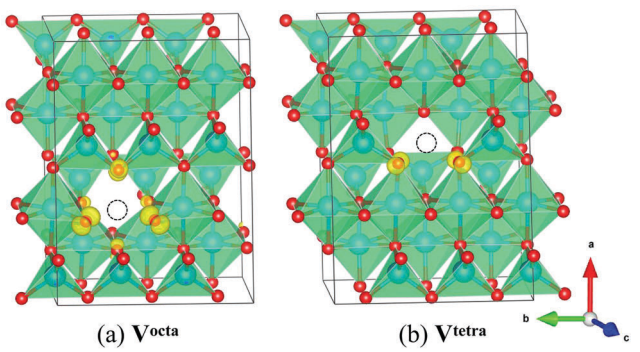

Fig. 4 Spin charge density of the surrounding O^{2-} anions of (a) V^{octa} and (b) V^{tetra}. The isosurface level is 0.033 e Å^{-3}. Larger blue and smaller red balls represent the Ga and O atoms, respectively. The dotted-line circles represent the Ga atoms which have been taken off.

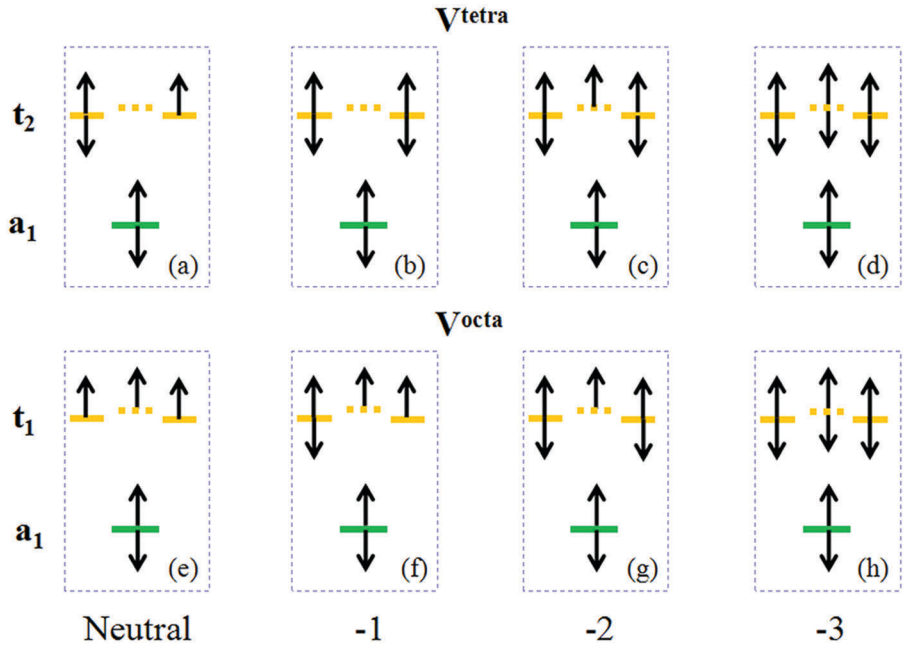

Fig. 5 Molecular orbitals and spin configurations diagram of defective Ga_2O_3 containing an isolated (a)–(d) four-fold coordinated Ga vacancy (V^{tetra}) and (e)–(h) six-fold coordinated Ga vacancy (V^{octa}) in various charge states. The dotted lines mark the partially occupied states which may induce the half-metal states of the systems.

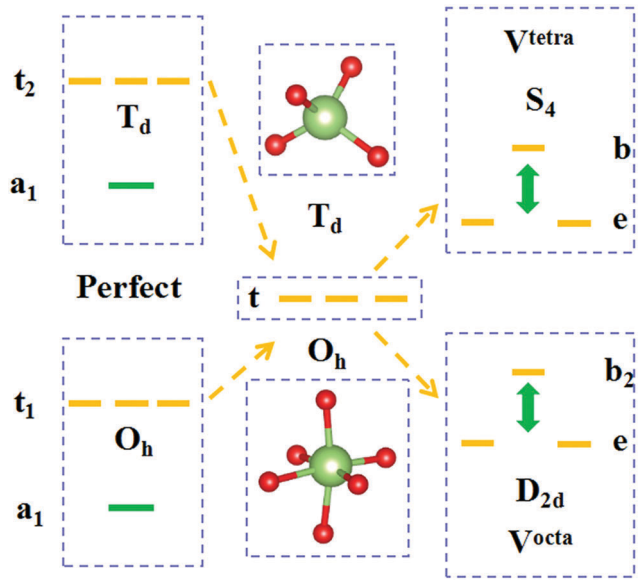

Fig. 6 The schematic diagram of the triply degenerate t levels which reduce to the double e orbitals and single b orbital for the distorted local structure around the vacancy. The red balls represent the O^{2-} anions and the green balls represent the Ga^{3+} cations.

the character table of the S_4 group, we can deduce the new molecular orbitals:

$$a_1:\ v=\frac{1}{2}\left(\psi_1'+\psi_2'+\psi_3+\psi_4\right) \quad (10)$$

$$e:\ t_x=\frac{1}{2}\left(\psi_1'-\psi_2'-\psi_3+\psi_4\right) \quad (11)$$

$$t_y=\frac{1}{2}\left(\psi_1'-\psi_2'+\psi_3-\psi_4\right) \quad (12)$$

$$b:\ t_z=\frac{1}{2}\left(\psi_1'+\psi_2'-\psi_3-\psi_4\right) \quad (13)$$

Taking into account the spin charge density in Fig. 4(b), we suggest that two of the four atomic orbitals (ψ_3 and ψ_4) are similar to the ones for the perfect T_d group in V^{tetra} with S_4 symmetry. The ψ_1' and ψ_2' are located on the O1 and O2 atoms (in Fig. 1c). The results suggest that the t_x and t_y are degenerate with the double e orbitals, and the t_z level is lifted as a high energy single b orbital.

Similarly, for the V^{octa} with the D_{2d} group, the molecular orbitals are changed as:

$$a_1:\ v=\frac{1}{\sqrt{6}}\left(\psi_1+\psi_2+\psi_3+\psi_4+\psi_5+\psi_6'\right) \quad (14)$$

$$e:\ t_x=\frac{1}{\sqrt{2}}(\psi_1-\psi_2) \quad (15)$$

$$t_y=\frac{1}{\sqrt{2}}(\psi_3-\psi_4) \quad (16)$$

$$b_2:\ t_z=\frac{1}{\sqrt{2}}\left(\psi_5-\psi_6'\right) \quad (17)$$

According to Fig. 4(a), the ψ_6' on the top O atom is deviated from the ψ_6 in the O_h group. So we can get a higher energy level with b_2 symmetry. The remaining two levels are degenerate as a double e orbital.

Therefore, going back to the DOS of the V^{tetra} and V^{octa}, we can explain that: (1) the s-like a levels are located deeply in the valence band and thus fully filled. The t levels would retain the neutral state if three electrons are introduced there. (2) For the V^{octa} system, the half-filled t_1 level leads to a half-metal-like state above the Fermi level in one spin channel and achieves a "high spin" state. (3) For the V^{tetra} system, the symmetry-breaking t level allows the electrons to configure a relatively low spin state resulting in a totally empty b level, corresponding to the defect level in the gap and also a weaker half-metal-like state in the e level. As shown in Fig. 3(c) and (d), the red circle marks the empty b level in the gap for the defect states of the V^{tetra} system and the blue stars indicate the partially occupied states in the spin down channel responsible for half-metal-like states. In this way, we clearly illustrate the different behaviors of V^{tetra} and V^{octa}, and especially why the defect states only appear in the V^{tetra} system.

To further test our theory, we calculate the magnetic properties involving the two different vacancy systems with different charge states as shown in Fig. 7. In detail, the moment of the V^{octa} is monotonously reduced with the increase of the charge states from the neutral to the −3 charged state. However, the moments of the V^{tetra} have some oscillation *vs.* the charge states. It can be concluded that for the −3 charge state both the two vacancy systems which are introduced by 3 electrons will be completely compensated, giving rise to a nonmagnetic state just like the pure Ga_2O_3. To explain this, we analyze the molecular orbitals of the V^{tetra} and V^{octa} as shown in Fig. 5(a)–(h). For the V^{octa}, the introduced electrons will occupy the empty states in the down spin channel one by one. In this process, the uncompensated spins vary from 3 (neutral) to 2 (−1 charged), to 1 (−2 charged) and eventually to the 0 (−3 charged) nonmagnetic state. In contrast, for the V^{tetra} case the first introduced electron would preferentially occupy the lower e level, forming a nearly nonmagnetic state for the −1 charged vacancy. Then, a second electron in the system would fill the highest b level and generate a one spin state for the −2 charge state. Finally, a nonmagnetic state of the completely-filled t_2 level is for the −3 charge state. Therefore, we can well connect the magnetic behaviors with the molecular orbitals and get the correct spin configurations for different charged states. Indeed, as shown in Fig. 7, there is a quantitative difference between the values from first-principles calculations (GGA+*U* and HSE06) and those deduced from molecular orbital theory. The calculation with a bigger supercell containing 120 atoms (119 atoms for the vacancy structure) confirmed that this is an intrinsic phenomenon originating from the half-metal states of the systems as shown in the Fig. 3. In agreement with the literature, the half-metal states are formed for some partially occupied molecular orbitals. For example, in HfO_2 the magnetic moment was found to be 3.5 μ_B per vacancy which is smaller than the 4 μ_B from molecular orbital theory for the half-metal state in the down spin states.[4] Additionally, in CaO the partially occupied e state also leads to a smaller spin moment than predicted from theory.[56] The numerically calculated spin moment on the orbital might be more delocalized than the values based on molecular theory. Therefore, for the intrinsic partially occupied states, we obtain the same trend of spin moments using DFT for different charge states compared with the theoretical model. The molecular orbitals with the higher energy levels, namely the b (or b_2) orbital, are thus hinted to be the partially occupied ones with about 60% population.

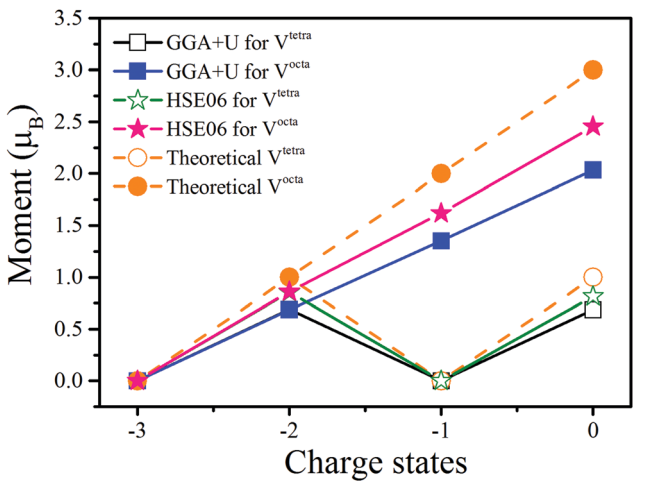

Fig. 7 The local moments induced by the V^{tetra} and V^{octa} defects in different charge states.

3.4 The long range magnetic order

The single isolated vacancy indeed induces some local spin moments around its location. For application purposes, it is necessary to verify the possible long range magnetic ordering in the vacancy systems. So we constructed a bigger supercell (120 atoms) consisting of two neutral Ga vacancies (for the V^{tetra} pair and V^{octa} pair) which are separated by a distance of 9.111 Å. By using different initial settings of magnetic moments calculated with U_{Ga-s} = 30 eV, we obtain and compare the two magnetic states namely the ferromagnetic (FM) and antiferromagnetic (AFM) cases. As summarized in Table 1, the FM states have a net moment of 1.368 μ_B for the two V^{tetra} and 4.068 μ_B for the two V^{octa}. Then, the stable state for the two V^{tetra} is the FM state while for the two V^{octa} the stable state is the AFM state. The energy differences ($\Delta E = E_{AFM} - E_{FM}$) are about 55.0 meV ($V^{tetra}$) and −16.0 meV ($V^{octa}$) respectively, from which we can estimate the corresponding critical transition temperature T_C by the Heisenberg model $H = -\sum_{i,j} Jm_i m_j$.[14] In the mean field approximation, the T_C values are calculated as $2k_BT_C = 3J_0$. The nearest-neighbor exchange parameter J_0 can be calculated as

Table 1 The more stable magnetic order, net moment, energy differences ($\Delta E = E_{AFM} - E_{FM}$), nearest-neighbor exchange parameter J_0 and transition temperature T_C (estimated from $2k_BT_C = 3J_0$) for the 120-atom supercells with a vacancy separation of 9.111 Å

Vacancy-type	Stable order	Net moment (μ_B)	ΔE (meV)	J_0 (meV)	T_C (K)
V^{tetra}	FM	1.371	55.0	55.0	963.8
V^{octa}	AFM	4.069	93.5	−1.2	20.9

$J_0 = \Delta E/nS^2$ (n = 4 for V^{tetra} and n = 6 for V^{octa}). As a result, the calculated values of J_0 and T_C for the two V^{tetra} system indicate that a long-range FM order may exist at room temperature. However, for the different ground-states of the two V^{octa} or two V^{tetra}, the magnetic interaction may be very complex in bulk with many vacancies in reality. Considering this competition between the FM and AFM, it may be challenging to observe the magnetism of β-Ga_2O_3 in experiments.

4. Conclusion

In summary, we have investigated the Ga cation vacancy defects states in β-Ga_2O_3 and the electronic structures from first principles calculations. At two different Ga sites, namely the four-fold coordinated and the six-fold coordinated ones, we identified that both the cation vacancies could result in a spin polarization originating from the local moments of surrounding O^{2-} anions. Using molecular orbital theory, we analysed the effects of the local symmetry on the vacancy states and obtained a picture of the magnetic configurations with possible charge states. It is obvious that the magnetic behaviors could be connected with the different electron occupations of the molecular orbitals. In addition, we also investigated the coexistence and interaction between the two cation vacancies. The computational solution of the magnetic orders and nearest-neighbor exchange parameters indicate a room temperature long-range ferromagnetic order.

Conflicts of interest

There are no conflicts of interest to declare.

Acknowledgements

This work is supported by the National Natural Science Foundation of China (No. 51372149, 51672171, 11574194, 11547011), the National Key Basic Research Program of China (Grant No. 2015CB921600), QiMingXing (No. 14QA1402000) and a research grant (No. 16DZ2260600) of the Shanghai Municipal Science and Technology Commission, Eastern Scholar Program, and the Shuguang Program (Grant No. 12SG34) from the Shanghai Municipal Education Commission. The Special Program for Applied Research on Super Computation of the NSFC-Guangdong Joint Fund (the second phase), the supercomputing services from AM-HPC, and the Shanghai Supercomputer Center are also acknowledged.

References

1 J. M. D. Coey, *Solid State Sci.*, 2005, **7**, 660–667.
2 M. Venkatesan, C. B. Fitzgerald and J. M. D. Coey, *Nature*, 2004, **430**, 630.
3 H. Weng and J. Dong, *Phys. Rev. B: Condens. Matter Mater. Phys.*, 2006, **73**, 132410.
4 C. D. Pemmaraju and S. Sanvito, *Phys. Rev. Lett.*, 2005, **94**, 217205.
5 K. P. McKenna and D. M. Ramo, *Phys. Rev. B: Condens. Matter Mater. Phys.*, 2015, **92**, 205124.
6 B. Y. Zhang, B. Yao, Y. F. Li, A. M. Liu, Z. Z. Zhang, B. H. Li, G. Z. Xing, T. Wu, X. B. Qin, D. X. Zhao, C. X. Shan and D. Z. Shen, *Appl. Phys. Lett.*, 2011, **99**, 182503.
7 M. Venkatesan, C. B. Fitzgerald, J. G. Lunney and J. M. D. Coey, *Phys. Rev. Lett.*, 2004, **93**, 177206.
8 T. Chanier, I. Opahle, M. Sargolzaei, R. Hayn and M. Lannoo, *Phys. Rev. Lett.*, 2008, **100**, 026405.
9 B. Roul, M. K. Rajpalke, T. N. Bhat, M. Kumar, A. T. Kalghatgi, S. B. Krupanidhi, N. Kumar and A. Sundaresan, *Appl. Phys. Lett.*, 2011, **99**, 162512.
10 S. W. Fan, K. L. Yao, Z. L. Liu, G. Y. Gao, Y. Min and H. G. Cheng, *J. Appl. Phys.*, 2008, **104**, 043912.
11 Z. Zhang, U. Schwingenschlögl and I. S. Roqan, *J. Appl. Phys.*, 2014, **116**, 183905.
12 T. Mattila and R. M. Nieminen, *Phys. Rev. B: Condens. Matter Mater. Phys.*, 1997, **55**, 9571.
13 H. Jin, Y. Dai, B. B. Huang and M.-H. Whangbo, *Appl. Phys. Lett.*, 2009, **94**, 162505.
14 X. Wang, M. Zhao, T. He, Z. Wang and X. Liu, *Appl. Phys. Lett.*, 2013, **102**, 062411.
15 R. J. Green, T. Z. Regier, B. Leedahl, J. A. McLeod, X. H. Xu, G. S. Chang, E. Z. Kurmaev and A. Moewes, *Phys. Rev. Lett.*, 2015, **115**, 167401.
16 K. Matsunaga, Y. Tanaka, K. Toyoura, A. Nakamura, Y. Ikuhara and N. Shibata, *Phys. Rev. B: Condens. Matter Mater. Phys.*, 2014, **90**, 195303.
17 D. Berger, H. Oberhofer and K. Reuter, *Phys. Rev. B: Condens. Matter Mater. Phys.*, 2015, **92**, 075308.
18 P. Deák, B. Aradi and T. Frauenheim, *Phys. Rev. B: Condens. Matter Mater. Phys.*, 2015, **92**, 045204.
19 G. Pacchioni, *Solid State Sci.*, 2000, **2**, 161.
20 P. Deák, L. C. Snyder, R. K. Singh and J. W. Corbett, *Phys. Rev. B: Condens. Matter Mater. Phys.*, 1987, **36**, 9612.
21 A. S. Zyubin, A. M. Mebel and S. H. Lin, *J. Phys. Chem. A*, 2007, **111**, 9479.
22 J. Paier, C. Penschke and J. Sauer, *Chem. Rev.*, 2013, **113**, 3949.
23 K. C. Snyder and W. B. Fowler, *Phys. Rev. B: Condens. Matter Mater. Phys.*, 1993, **48**, 13238.
24 A. Shluger, E. Kotomin and Y. Dzelme, *Phys. Status Solidi B*, 1979, **96**, 91.
25 K. J. Børve, *J. Chem. Phys.*, 1991, **95**, 4626.
26 A. De Vita, M. J. Gillan, J. S. Lin, M. C. Payne and I. Štich, *Phys. Rev. B: Condens. Matter Mater. Phys.*, 1992, **46**, 12964.
27 L. Ojamäe and C. Pisani, *J. Chem. Phys.*, 1998, **109**, 10984.
28 Y. H. Hu and E. Ruckenstein, *J. Chem. Phys.*, 2004, **120**, 7971.
29 I. S. Elfimov, S. Yunoki and G. A. Sawatzky, *Phys. Rev. Lett.*, 2002, **89**, 216403.
30 M. Mohamed, C. Janowitz, I. Unger, R. Manzke, Z. Galazka, R. Uecker, R. Fornari, J. R. Weber, J. B. Varley and C. G. Van de Walle, *Appl. Phys. Lett.*, 2010, **97**, 211903.

31 V. Sridharan, S. Banerjee, M. Sardar, S. Dhara, N. Gayathril and V. S. Sastry, 2007, arXiv:cond-mat/0701232v1.
32 M. M. Branda, S. E. Collins, N. J. Castellani, M. A. Baltanás and A. L. Bonivardi, *J. Phys. Chem. B*, 2006, **110**, 11847–11853.
33 J. B. Varley, J. R. Weber, A. Janotti and C. G. Van de Walle, *Appl. Phys. Lett.*, 2010, **97**, 142106.
34 P. Deak, Q. D. Ho, F. Seemann, B. Aradi, M. Lorke and T. Frauenheim, *Phys. Rev. B*, 2017, **95**, 075208.
35 L. Dong, R. Jia, B. Xin, B. Peng and Y. Zhang, *Sci. Rep.*, 2017, **7**, 40160.
36 X. Ma, Y. Zhang, L. Dong and R. Jia, *Results Phys.*, 2017, **7**, 1582.
37 A. N. Kocharian, G. W. Fernando, K. Palandage and J. W. Davenport, *Phys. Rev. B: Condens. Matter Mater. Phys.*, 2006, **74**, 024511.
38 A. N. Kocharian, G. W. Fernando, K. Palandage and J. W. Davenport, *Phys. Rev. B: Condens. Matter Mater. Phys.*, 2008, **78**, 075431.
39 G. Kresse and J. Hafner, *Phys. Rev. B: Condens. Matter Mater. Phys.*, 1993, **47**, 558.
40 G. Kresse and J. Hafner, *J. Phys.: Condens. Matter*, 1994, **6**, 8245.
41 G. Kresse and J. Furthmller, *Phys. Rev. B: Condens. Matter Mater. Phys.*, 1996, **54**, 11169.
42 S. L. Dudarev, G. A. Botton, S. Y. Savrasov, C. J. Humphreys and A. P. Sutton, *Phys. Rev. B: Condens. Matter Mater. Phys.*, 1998, **57**, 1505.
43 J. P. Perdew, K. Burke and M. Ernzerhof, *Phys. Rev. Lett.*, 1996, **77**, 3865.
44 J. P. Perdew, J. A. Chevary, S. H. Vosko, K. A. Jackson, M. R. Pederson, D. J. Singh and C. Fiolhais, *Phys. Rev. B: Condens. Matter Mater. Phys.*, 1992, **46**, 6671.
45 T. R. Paudel and W. R. L. Lambrecht, *Phys. Rev. B: Condens. Matter Mater. Phys.*, 2008, **77**, 205202.
46 T. R. Paudel and W. R. L. Lambrecht, *Phys. Status Solidi B*, 2011, **248**, 1043.
47 M. Yamaga, E. G. Víllora, K. Shimamura, N. Ichinose and M. Honda, *Phys. Rev. B: Condens. Matter Mater. Phys.*, 2003, **68**, 155207.
48 P. E. Blöchl, O. Jepsen and O. K. Andersen, *Phys. Rev. B: Condens. Matter Mater. Phys.*, 1994, **49**, 16223.
49 A. V. Krukau, O. A. Vydrov, A. F. Izmaylov and G. E. Scuseria, *J. Chem. Phys.*, 2006, **125**, 224106.
50 J. Heyd and G. E. Scuseria, *J. Chem. Phys.*, 2004, **121**, 224106.
51 C. Freysoldt, B. Grabowski, T. Hickel, J. Neugebauer, G. Kresse, A. Janotti and C. G. Van de Walle, *Rev. Mod. Phys.*, 2014, **86**, 253.
52 C. Mitra, C. Lin, J. Robertson and A. A. Demkov, *Phys. Rev. B: Condens. Matter Mater. Phys.*, 2012, **86**, 155105.
53 A. A. Demkov, *Phys. Rev. B: Condens. Matter Mater. Phys.*, 2006, **74**, 085310.
54 P. Dev, Y. Xue and P. Zhang, *Phys. Rev. Lett.*, 2008, **100**, 117204.
55 SymApps 6.0 for Windows Bio-Rad Laboratories, Sadtler Division, 3316 Spring Garden St., Philadelphia, PA.
56 J. Osorio-Guillén, S. Lany, S. V. Barabash and A. Zunger, *Phys. Rev. Lett.*, 2006, **96**, 107203.